PROCEEDINGS OF SCIENCE

Towards $Wb\bar{b}+j$ at NLO with NLOX

Laura Reina*
Florida State University, Keen Building, Tallahassee, FL 32306-4350, USA
E-mail: reina@hep.fsu.edu

Thomas Schutzmeier
Florida State University, Keen Building, Tallahassee, FL 32306-4350, USA
E-mail: tschutzmeier@gmail.com

We review our calculation of the $\mathcal{O}(\alpha_s)$ virtual corrections to $qg \to Wb\bar{b}q'$ obtained with NLOX, a new automatized approach to the evaluation of one-loop amplitudes in terms of Feynman diagrams, and discuss its physical relevance.

Loops and Legs in Quantum Field Theory - 11th DESY Workshop on Elementary Particle Physics, April 15-20, 2012
Wernigerode, Germany

*Speaker.

PoS(LL2012)021

1. Introduction

The associated production of a W boson with a pair of massive bottom quarks, contributing to both the $W+b$-jet and $W+2\,b$-jet signatures, represents one of the most important background processes in searching for a light Higgs boson as well as single-top production. The precise theoretical knowledge of these processes provides moreover an excellent probe of the current understanding of QCD in various kinematic regimes at high-energy hadron colliders.

The cross sections for W boson + b jets production have been measured at the Tevatron $p\bar{p}$ collider at Fermilab by both the CDF [1] and D0 [2] collaborations, and more recently at the Large Hadron pp Collider (LHC) at CERN by the ATLAS collaboration [3]. New measurements with better statistics are expected soon from both ATLAS and CMS.

On the theoretical side, next-to-leading order (NLO) QCD corrections to W production with up to two jets containing at most one heavy b jet are known [4] and cross sections for $W+2\,b$-jets were determined both in the massless b-quark approximation [5, 6, 7, 8, 9] and including b-quark mass effects [10, 11, 12, 13] at the same level of precision. From existing NLO QCD calculations, the theoretical prediction for the production of $W+2$ jets with at least one b jet has been provided in Ref. [14] and compared to the CDF [1] and ATLAS [3] measurements in Refs. [15] and [16] respectively. Furthermore, the NLO calculation of $Wb\bar{b}$ has been interfaced with parton-shower Monte Carlo generators using both the `POWHEG` [17] and the `MC@NLO` [18] methods.

As shown in Ref. [12], the NLO theoretical prediction for $Wb\bar{b}$ production still suffers from large renormalization and factorization scale uncertainties in particular at the LHC. In fact, at this order of perturbative QCD, a new qg initiated channel with an additional parton in the final state ($qg\to Wb\bar{b}q'$) opens up and, being a tree level process, introduces a strong scale dependence. This effect is particularly pronounced at the LHC, where the NLO qg channel competes with the $q\bar{q}'$ channel due to the substantial initial state gluon density. Only a complete NNLO calculation of $pp(p\bar{p})\to Wb\bar{b}$ can be expected to reduce this spurious scale dependence and give a theoretical prediction consistent at this order of QCD. This clearly represents an extremely challenging problem that needs to be solved in steps, and will probably require several new developments to extend the reach of currents techniques.

In a recent paper [19] we have presented results for one of the many contributions to $pp(p\bar{p})\to Wb\bar{b}$ at NNLO: the $\mathcal{O}(\alpha_s)$ virtual corrections to the $qg\to Wb\bar{b}q'$ channel, keeping the full bottom-quark mass dependence[1]. Indeed, this contribution is particularly interesting for two main reasons. First of all, the $\mathcal{O}(\alpha_s)$ virtual corrections to the $qg\to Wb\bar{b}q'$ channel are a well-defined independent piece of the overall NNLO calculation of $Wb\bar{b}$ hadroproduction. When combined with the $\mathcal{O}(\alpha_s)$ virtual corrections to $q\bar{q}'\to Wb\bar{b}g$ (obtained from the same calculation by crossing of initial and final states), they provide a self-standing and well-defined part of the one-loop contributions to the full NNLO $Wb\bar{b}$ cross section, namely the one-loop virtual contributions from $2\to 4$ processes. Furthermore, when complemented with the corresponding real corrections to $qg\to Wb\bar{b}q'$ and $q\bar{q}'\to Wb\bar{b}g$, our calculation completely determine the NLO cross sections for both $Wb\bar{b}+j$ and, within a fully consistent four-flavor-number scheme, $Wb+j$ production, i.e. for the production of a W boson with one or two b jets plus a light jet, where the difference between the two processes is

[1] Results for the $\bar{q}g\to Wb\bar{b}\bar{q}'$ channel are identical at the partonic level and in the following it will be understood that $qg\to Wb\bar{b}q'$ refers to both channels.

just the number of b jets tagged in the final state (the parton level processes being the same in the four-flavor-number scheme). Since NLO real-emission contributions nowadays can be determined in a mostly automatized fashion with the help of existing packages, for instance SHERPA [20], as well as NLO Monte Carlo frameworks as POWHEG [21, 22] and MC@NLO [23], the virtual one-loop corrections that we have calculated [19] constitute the only missing piece for the NLO QCD cross section prediction of the above processes and are therefore highly desirable. They should indeed contribute to reduce the theoretical uncertainty from the unphysical scale dependence that plague the prediction of $W+b$-jets cross sections.

In recent years, prompted by the increasing complexity of multi-particle one-loop calculations, two different strategies have been primarily developed for the evaluation of one-loop corrections: the traditional Feynman-diagram-based approach as well as unitarity techniques [32, 33]. Powerful packages like BlackHat [34, 25], CutTools [35], Helac-nlo [36], Rocket [37, 27] and MadLoop [38] exist that provide automatization and efficient numerical implementations of unitarity methods and that have been successfully applied to the calculation of cutting-edge one-loop processes. Recently, the automatized package GoSam [39] has been developed and applied to the automatized computation of a wide range of NLO cross sections. Moreover, several fast and efficient private codes exist that follow the traditional approach of Feynman diagrams and tensor-integral reduction.

To accomplish our task, we have developed a new independent automatized approach to one-loop calculations based on Feynman diagrams, that we have encoded in a package, NLOX, to be eventually released for public use. We have tested our techniques against several $2\to 3$ and $2\to 4$ processes for which results are available. For instance, we have been able to reproduce the $\bar{u}d\to Wd\bar{d}g$ results for $W+3\,j$ production at NLO [26, 24], and we have cross-checked parts of the one-loop corrections to the cross section of $qg\to Wb\bar{b}q'$ with results provided by the GoSam collaboration.

In these proceedings we will review the main characteristics of our approach with particular focus on the general strategy used to generate and simplify amplitude-specific expressions as well as to implement a numerically stable evaluation of one-loop tensor integrals. We will conclude by presenting a numerical result for $dg\to Wb\bar{b}u$ at NLO for a single phase-space point and by discussing the analysis of the achieved accuracy and computation times.

2. General strategy

At leading order in the strong coupling, the $qg\to Wb\bar{b}q'$ process, with the choice $q=d$ and $q'=u$ which we consider in the following, consists of 12 tree level diagrams. Examples of these diagrams are depicted in fig. 1 and one-loop QCD corrections are obtained by adding virtual gluons and fermions, yielding 308 Feynman diagrams. Ultra-violet (UV) and infrared (IR) divergences are regularized with dimensional regularization in $d=4-2\varepsilon$ dimensions and we keep the full bottom-quark mass dependence while lighter quarks are treated as massless. We enforce transversality of external bosons through $p_W\cdot\varepsilon_W=0$ and $p_g\cdot\varepsilon_g=0$, with $\varepsilon^\mu_{W/g}$ and $p^\mu_{W/g}$ being the polarization vectors and momenta of the W boson and gluon, respectively. While this choice is obvious for gluons, it is justified for the W boson only for weak couplings to massless fermions, which is the case in the amplitude at hand.

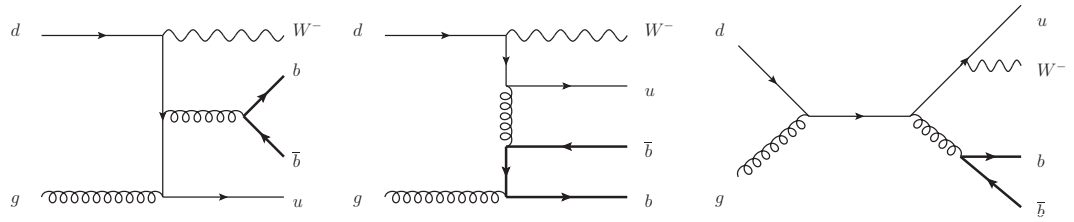

Figure 1: Example of LO diagrams for $dg \to Wb\bar{b}u$.

In the traditional Feynman diagram based approach to the evaluation of one-loop corrections, a given NLO amplitude $\mathscr{M}^{(1)}$ is commonly decomposed as

$$\mathscr{M}^{(1)} = \sum_i C_i \sum_j c_{ij} I_j \hat{\mathscr{M}}_j^{(1)} \tag{2.1}$$

with color structures C_i and polarization/spin information $\hat{\mathscr{M}}_j^{(1)}$. I_j denotes tensor one-loop integrals after decomposition into tensor structures of external momenta and contraction of all Lorentz indices. The sum over j in eqn. (2.1) for a given term C_i runs over all one-loop sub-diagrams with the same color structure.

The color- and spin-summed and/or -averaged squared amplitude is given by

$$\Gamma = \mathrm{Re}\left(\sum_{\text{colors pol}} \sum \mathscr{M}^{(1)} \mathscr{M}^{(0)*} \right) = \mathrm{Re}\left(\sum_n I_n \Lambda_n \right) \tag{2.2}$$

with

$$\Lambda_n = \sum_{ij} \sum_{colors} C_i C_j^* \sum_{pol} c_{in} \hat{\mathscr{M}}_n^{(1)} \hat{\mathscr{M}}_j^{(0)*} \tag{2.3}$$

where $\mathscr{M}^{(0)}$ is the leading-order amplitude

$$\mathscr{M}^{(0)} = \sum_i C_i \hat{\mathscr{M}}_i^{(0)}, \tag{2.4}$$

decomposed in color space on the same basis of color structures C_i.

After organizing the NLO amplitude by color factor, standard $SU(3)$ relations are applied to simplify the color structures and the resulting set of color coefficients is extracted. Summing/averaging over final/initial color indices, after contraction with the LO color components, yielding the $C_i C_j^*$ term in eqn. (2.3), is performed at this point. In the next step, tensor integrals are decomposed into Lorentz invariant tensor coefficients and a standard ordering of Dirac and spinor structures is achieved with the help of anti-commutation relations of Dirac matrices and the application of the equations of motion. The amplitude is subsequently expanded in $(d-4)$ and UV/IR divergences are separated such that four-dimensional identities can be safely used without introducing the need for rational terms of either IR or UV origin [29]. Moreover, this approach also avoids ambiguities in the definition of the γ_5 matrix, which we treat in naive dimensional regularization.

The complete polarization information of the amplitude is contained in Dirac chains and polarization vectors of external bosons, commonly called standard matrix elements (SME), $\hat{\mathscr{M}}_k$. At

this stage, the number of SME is of the order of several thousand for both $2 \to 4$ processes. Reducing the set of SME to linear combinations in a smaller basis $\{\tilde{\mathscr{M}}_k\}$ is crucial since the size of final expressions, and therefore the computational complexity, scales with the number of SME. Algebraic relations based on four-dimensional identities tailored for the specific process and SME at hand have been described in [41, 40, 29, 30, 31] and successfully applied in several calculations. To automatize this procedure, we have developed a graph based approach to the SME reduction that allows for an efficient implementation and performs a brute-force search for a small SME basis. Products of Dirac chains are translated to directed graphs where the various structures, like gamma matrices, projection operators, and spinors are represented by nodes, and directed edges describe contractions of Lorentz indices and the ordering of structures. Algebraic relations then translate to operations on graphs, for instance shrinking of edges, exchanging or adding of nodes, and result in general in disconnected graphs. Since this method can be expressed very efficiently within the framework of graph theory without the need for computationally expensive algebraic manipulations of lengthy expressions, our implementation is capable of testing a huge number of combinations of transformations. Typically, the original set of SME is reduced to a basis of several hundred elements this way. Our variant of the SME reduction is discussed in more detail in Ref. [42].

On the other hand, the general strategy for the evaluation of tensor integrals coefficients is their reduction to master integrals, usually scalar N-point functions T_0^N. In the case of N-point tensors with $N \leq 4$ the well-known Passarino-Veltman (PV) algorithm [43] can be used, while $N > 4$ coefficients are reduced to linear combinations of four-point tensor integrals. Due to numerical instabilities in the vicinity of phase-space points where Gram determinants become small, alternative reduction techniques exist to produce reliable results.

Our tensor reduction approach combines different methods, allows for cross checks between them and ensures numerical stability in an automatized way. For N-point functions with $N \leq 4$ the following reduction schemes are used:

- PV reduction [43],
- reduction with modified Cayley determinants as introduced by Denner and Dittmaier (DD) in [44], and
- expansions around small quantities, like Gram/Cayley determinants and kinematic invariants (DDx) developed by the same authors of Ref. [44].

In addition, our software is capable of producing multiple precision (MP) reductions with help of the `qd` library [45], that turn out to be numerically stable already in the framework of the PV reduction (MP PV). Tensor coefficients with five and six external legs are evaluated following an approach by Diakonidis et al. [46, 47] that is free of inverse Gram determinants (GDF) and therefore numerically stable.

Our implementation is inspired by [44] and performs the reduction numerically. However, the original recursive algorithm is unrolled into an iterative procedure by arranging the tensor coefficients in a tree-like structure, which provides fine-grained control over different aspects of the reduction. We choose the PV reduction for $N \leq 4$ in the absence of numerical instabilities and the GDF reduction for $N > 4$ as our standard methods. Based on these reductions, the evaluation tree

is constructed for the required set of tensor coefficients in such a way that the minimal number of evaluations is guaranteed. For optimal reuse of intermediate results, coefficients with different mass distributions on internal propagators are brought to a standard form with respect to the external momenta and internal masses and are treated together. As already mentioned, this strategy works well in large regions of phase space, but becomes numerically unstable if small Gram determinants in $N \leq 4$ point coefficients are encountered. In this case, the evaluation tree is extended with subtrees for the unstable tensor functions and their dependencies only. These newly created subtrees are computed with one of the alternative methods, either DD or DDx as needed, or with MP PV, to ensure numerical stability, while all other nodes are reduced with the default procedures. While both approaches provide numerically stable results, we use the former techniques mainly for cross checks in critical phase-space regions while we employ the latter in computations of squared amplitudes. As subtrees are added, the reduction program keeps track of the conditions that lead to inconsistencies such that the newly created evaluation paths can be reused in future evaluations.

As a last step, the products $\mathscr{M}_n^{(1)}\mathscr{M}_k^{(0)*}$ of the NLO SME with the leading-order color amplitudes are evaluated, Dirac chains properly contracted, and summations over spins and polarizations as well as traces are performed. We translate the resulting expressions into `C` code for an efficient numerical evaluation.

It is important to note that in `NLOX`, after specifying the desired process and kinematics, no user interaction is required from the point of diagram generation to the final numerical code for the cross section evaluation at single phase-space points. All algebraic manipulations are performed using `FORM` while other components like SME and tensor reductions are developed in `C++`. Transparent interfaces, using `Python`, process input and output between the different stages and allow for extensive intermediate checks. The final cross section evaluation is made accessible through an automatically generated and flexible `C++` interface that allows, for instance, the evaluation of single diagrams or color amplitudes interfered with the LO contributions, the extraction of divergences, different reduction methods or a direct connection with a phase-space generator.

3. Results

A big component of developing the `NLOX` package deals with controlling numerical instabilities. Detecting numerical instabilities at a single phase-space point is in general a non-trivial task without examining the surrounding phase-space domain or additional external information. Performing the tensor reduction in $d = 4 - 2\varepsilon$ dimensions and regulating both ultraviolet and infrared divergences dimensionally, however, offers a direct handle on the achieved accuracy. Firstly, the scalar one-loop integrals in terms of which the tensor-integral coefficients are reduced have to be known retaining the full pole structure. For this task, we use a custom implementation based on `QCDLoop` [48] for the IR poles together with a modified version of `LoopTools` [49] that allows for multiple precision evaluations. During the reduction which is performed on the divergent and finite parts separately, UV/IR poles are affected by the same numerical instabilities as the finite part. Provided the divergences can be computed for a given tensor coefficient independently in a reliable way, a direct comparison can be used to detect a loss of precision[2]. UV poles of tensor coefficients

[2] At the cross section level, the same approach to identify numerical instabilities has been successfully used in [34, 50, 26].

in the minimal subtraction scheme are mass independent and can either be obtained with a single analytic reduction or can be taken from the appendix of [44]. In contrast, IR divergences occur in certain limits of vanishing kinematic invariants and have to be studied in all these cases individually. To this end, we have reduced 3- and 4-point tensor coefficients up to rank 4 analytically in the various IR divergent limits. Using these results a numerically stable library for their computation was carefully established and thoroughly cross-checked with the full analytical results for a wide range of input parameters. In our reduction, the UV and IR poles of each tensor coefficient are then checked against this library for every phase-pace point and, in case of inconsistencies, alternative reduction methods are employed as described above.

If the stability check on the UV and IR pole parts can detect the presence of instabilities arising from the tensor reduction process for those parts of the amplitude that contain UV and IR singularities, and in these cases it is a necessary and sufficient SME reductions in automated NLO computations with NLOX"test, it will however miss instabilities arising from the terms that do not contain UV and IR singularities. In our Feynman-diagram-based approach we can isolate these cases, since they correspond to the contributions from finite Feynman diagrams. In these cases, instabilities from tensor integral reduction still can arise and we isolate them with a very simple-minded test that studies the oscillations of the amplitude square in a neighborhood of each phase-space point. If large oscillations are detected, the evaluation is switched to multiple precision.

Of course, this procedure comes with a computational cost, that is mainly due to the multiple reductions for pole and finite parts and the evaluation of scalar integrals, while the contribution from the IR pole evaluation routines are negligible. However, thanks to the efficient design of the reduction algorithm and extensive caching, the run times are competitive with what is reported in the literature: computation times in the numerically stable case for all tensor integrals required in a mixed massive and massless $2 \to 4$ process average at around 20 ms per phase-space point on an Intel i7 950 CPU at 3.07GHz.

Apart from instabilities in the reduction of tensor coefficients, cancellations in intermediate expressions of the unrenormalized squared amplitude Γ in eqn. (2.3) may also induce a loss of accuracy in some phase-space regions. Also instabilities may arise from the non-trivial analytic structure of the finite parts of the amplitude when the arguments of the logarithmic and dilogarithmic terms in it are pushed to limit regions of their arguments. The loss of precision is detected as explained in Sec. 2 and, in this case, we extend the numerical precision for both the complete tensor reduction as well as the evaluation of the whole contribution to Γ. This step is computationally most expensive, as a huge number of operations has to be performed in slow multiple precision mode both in the tensor reduction and in the evaluation of Γ. Fortunately, the proportion of this type of evaluations is in general relatively small. Compared to the naive approach where no analysis of instabilities is performed on the tensor reduction level, the necessary number of this kind of evaluations is substantially reduced.

Table 1 gives an overview of the obtained efficiency for the evaluation at $5 \cdot 10^4$ random phase-space points with reasonable cuts, requesting a maximal relative error of 10^{-5}. As expected, the evaluation time scales with the number of external particles. Moreover, due to a larger basis of SME, amplitudes containing weak couplings compared to for example $t\bar{t}\gamma$ production are computationally more expensive. An interesting observation, however, is the fact that the number of switches to multiple precision evaluations, both within the reduction and at the amplitude squared

Process	r_s	r_q	r_{dq}	t_m/ms	t_s/ms	t_q/ms	t_{dq}/ms	t_q^{full}/ms
$q\bar{q} \to \gamma t\bar{t}$	99.6%	0.4%	0	9.5	8.9	153	0	1069
$gg \to \gamma t\bar{t}$	98.9%	1.1%	0	12.0	10.1	182	0	1972
$q\bar{q}' \to Wb\bar{b}$	99.7%	0.3%	0	10.9	10.4	167	0	1264
$q\bar{q} \to Zb\bar{b}$	99.8%	0.1%	0.1%	17.7	14.4	217	3161	2290
$gg \to Zb\bar{b}$	98.3%	1.6%	0.1%	22.5	15.7	233	3314	2706
$\bar{u}d \to d\bar{d}gW$	95.4%	3.6%	1.0%	90.3	37.5	306	4358	5503
$ug \to b\bar{b}dW$	93.1%	5.6%	1.3%	95.4	29.7	311	3870	5192

Table 1: Benchmarks of the numerically stabilized method applied to various NLO amplitudes for the evaluation of $5 \cdot 10^4$ phase-space points. r_s, r_q and r_{dq} give the ratios of phase-space points that required either only standard (double) or also some additional quadruple/double-quadruple precision evaluations at the reduction or amplitude-squared level for reliable numerical results. t_m gives the mean evaluation time per phase-space point while t_s, t_q and t_{dq} denote separate mean timings for the respective numerical precision. Finally, the mean computation time of both the amplitude and tensor reduction in full quadruple precision is given in t_q^{full}. The above numbers were obtained on an Intel i7 950 CPU at 3.07GHz.

level, do not vary much between processes of comparable complexity. Although evaluations in quadruple precision take significantly more time with increasing number of external states, the overall evaluation time is governed by the numerically stable bulk of phase space.

For future reference, we provide our new result for the unrenormalized squared amplitude of $dg \to Wb\bar{b}u$ at NLO at a single phase-space point. The result is normalized to the LO cross section in the following way

$$\hat{\Gamma} = \frac{(4\pi)^{2-\varepsilon}}{8\pi\alpha_s} \frac{\Gamma(1-2\varepsilon)}{\Gamma(1+\varepsilon)\Gamma^2(1-\varepsilon)} \frac{\Gamma}{\left|\mathscr{M}^{(0)}\right|^2}, \tag{3.1}$$

such that the final result is independent of the strong and weak couplings as well as CKM matrix elements. Furthermore, we use

$$m_W = 80.41\,\text{GeVand} \tag{3.2}$$

$$m_b = 4.62\,\text{GeV}. \tag{3.3}$$

for the weak-boson and bottom-quark masses and set all external particles on-shell.

For $dg \to Wb\bar{b}u$ our result with $n_l = 4$ light and $n_h = 1$ heavy-quark flavors at the phase-space point of tab. 2 with renormalization scale $\mu^2 = (p_d + p_g)^2$ reads

$$\hat{\Gamma}(dg \to Wb\bar{b}u) = -5.6666667\,\varepsilon^{-2} + 39.342424\,\varepsilon^{-1} + 292.92493 \tag{3.4}$$

4. Conclusions

We have developed a new automatized approach to the evaluation of one-loop amplitudes in terms of Feynman diagrams (NLOX) and applied it to the calculation of the $\mathscr{O}(\alpha_s)$ virtual corrections to $qg \to Wb\bar{b}q'$ (and $q\bar{q}' \to Wb\bar{b}g$). These corrections enter the NNLO calculation of $Wb\bar{b}$ hadroproduction as well as the NLO calculation of both $Wb\bar{b}+j$ and $Wb+j$ production in a fully

	E	p^1	p^2	p^3
p_d	100.000000000000	0	0	100.000000000000
p_g	100.000000000000	0	0	−100.000000000000
p_u	14.4169546267975	−3.59819144566031	6.52544251406004	−12.3418069595668
p_b	53.6542637065835	−16.9076522158373	−49.1575349754512	12.4540622120327
$p_{\bar{b}}$	25.2318438952597	−17.2383739318242	−15.9080092164594	8.06692341047065
p_W	106.696937771359	37.7442175933219	58.5401016778506	−8.17917866293656

Table 2: Phase-space point used for $dg \to Wb\bar{b}u$

consistent four-flavor-number scheme. A thorough study of the impact of these corrections in both previous cases as well as the application of the method developed in this paper to other processes will be the subject of future publications.

References

[1] T. Aaltonen *et al.* [CDF Collaboration], Phys. Rev. Lett. **104**, 131801 (2010) [arXiv:0909.1505 [hep-ex]].

[2] V. M. Abazov *et al.* [D0 Collaboration], Phys. Rev. Lett. **94**, 091802 (2005) [arXiv:hep-ex/0410062].

[3] G. Aad *et al.* [ATLAS Collaboration], arXiv:1109.1470 [hep-ex].

[4] J. M. Campbell, R. K. Ellis, F. Maltoni and S. Willenbrock, Phys. Rev. D **75**, 054015 (2007) [arXiv:hep-ph/0611348].

[5] Z. Bern, L. J. Dixon and D. A. Kosower, Nucl. Phys. B **513**, 3 (1998) [arXiv:hep-ph/9708239].

[6] Z. Bern, L. J. Dixon, D. A. Kosower and S. Weinzierl, Nucl. Phys. B **489**, 3 (1997) [arXiv:hep-ph/9610370].

[7] R. K. Ellis and S. Veseli, Phys. Rev. D **60**, 011501 (1999) [arXiv:hep-ph/9810489].

[8] J. M. Campbell and R. K. Ellis, Phys. Rev. D **65**, 113007 (2002) [arXiv:hep-ph/0202176].

[9] J. M. Campbell, R. K. Ellis and D. L. Rainwater, Phys. Rev. D **68**, 094021 (2003) [arXiv:hep-ph/0308195].

[10] F. Febres Cordero, L. Reina and D. Wackeroth, Phys. Rev. D **74**, 034007 (2006) [arXiv:hep-ph/0606102].

[11] F. Febres Cordero, arXiv:0809.3829 [hep-ph].

[12] F. Febres Cordero, L. Reina and D. Wackeroth, Phys. Rev. D **80**, 034015 (2009) [arXiv:0906.1923 [hep-ph]].

[13] S. Badger, J. M. Campbell and R. K. Ellis, JHEP **1103**, 027 (2011) [arXiv:1011.6647 [hep-ph]].

[14] J. M. Campbell, R. K. Ellis, F. Febres Cordero, F. Maltoni, L. Reina, D. Wackeroth, S. Willenbrock, Phys. Rev. **D79**, 034023 (2009). [arXiv:0809.3003 [hep-ph]].

[15] F. F. Cordero, L. Reina and D. Wackeroth, PoS **RADCOR2009**, 055 (2010) [arXiv:1001.3362 [hep-ph]].

[16] F. Caola, J. M. Campbell, F. Febres Cordero, L. Reina and D. Wackeroth, Phys. Rev. **D86**, 034021 (2012). [arXiv:1107.3714 [hep-ph]].

[17] C. Oleari and L. Reina, JHEP **1108**, 061 (2011) arXiv:1105.4488 [hep-ph].

[18] R. Frederix, S. Frixione, V. Hirschi, F. Maltoni, R. Pittau and P. Torrielli, JHEP **1109**, 061 (2011) [arXiv:1106.6019 [hep-ph]].

[19] L. Reina and T. Schutzmeier, JHEP **1209**, 119 (2012) [arXiv:1110.4438 [hep-ph]].

[20] T. Gleisberg, S. Hoeche, F. Krauss, M. Schonherr, S. Schumann, F. Siegert and J. Winter, JHEP **0902**, 007 (2009) [arXiv:0811.4622 [hep-ph]].

[21] P. Nason, JHEP **0411**, 040 (2004). [arXiv:hep-ph/0409146 [hep-ph]].

[22] S. Frixione, P. Nason, C. Oleari, JHEP **0711**, 070 (2007). [arXiv:0709.2092 [hep-ph]].

[23] S. Frixione, B. R. Webber, JHEP **0206**, 029 (2002). [hep-ph/0204244].

[24] C.F. Berger, Z. Bern, Lance J. Dixon, F. Febres Cordero, D. Forde, T. Gleisberg, H. Ita, D.A. Kosower, D. Maitre Phys. Rev. D **82**, 074002 (2010) [arXiv:1004.1659 [hep-ph]].

[25] C.F. Berger, Z. Bern, Lance J. Dixon, F. Febres Cordero, D. Forde, T. Gleisberg, H. Ita, D.A. Kosower, D. Maitre Phys. Rev. Lett. **102**, 222001 (2009) [arXiv:0902.2760 [hep-ph]].

[26] C.F. Berger, Z. Bern, Lance J. Dixon, F. Febres Cordero, D. Forde, T. Gleisberg, H. Ita, D.A. Kosower, D. Maitre Phys. Rev. D **80**, 074036 (2009) [arXiv:0907.1984 [hep-ph]].

[27] R. K. Ellis, W. T. Giele, Z. Kunszt, K. Melnikov and G. Zanderighi, JHEP **0901**, 012 (2009) [arXiv:0810.2762 [hep-ph]].

[28] F. Campanario, ÂăÂăJHEP **1110** (2011) 070 ÂăÂă[arXiv:1105.0920 [hep-ph]]. ÂăÂă

[29] A. Bredenstein, A. Denner, S. Dittmaier and S. Pozzorini, JHEP **0808**, 108 (2008) [arXiv:0807.1248 [hep-ph]].

[30] A. Bredenstein, A. Denner, S. Dittmaier and S. Pozzorini, Phys. Rev. Lett. **103**, 012002 (2009) [arXiv:0905.0110 [hep-ph]].

[31] A. Bredenstein, A. Denner, S. Dittmaier and S. Pozzorini, JHEP **1003**, 021 (2010) [arXiv:1001.4006 [hep-ph]].

[32] Z. Bern, L. J. Dixon and D. A. Kosower, Annals Phys. **322**, 1587 (2007) [arXiv:0704.2798 [hep-ph]].

[33] R. K. Ellis, Z. Kunszt, K. Melnikov and G. Zanderighi, arXiv:1105.4319 [hep-ph].

[34] C. F. Berger *et al.*, Phys. Rev. D **78**, 036003 (2008) [arXiv:0803.4180 [hep-ph]].

[35] G. Ossola, C. G. Papadopoulos and R. Pittau, JHEP **0803**, 042 (2008) [arXiv:0711.3596 [hep-ph]].

[36] G. Bevilacqua, M. Czakon, M. V. Garzelli, A. van Hameren, A. Kardos, C. G. Papadopoulos, R. Pittau and M. Worek, ÂăÂăarXiv:1110.1499 [hep-ph]. ÂăÂă

[37] W. T. Giele and G. Zanderighi, JHEP **0806**, 038 (2008) [arXiv:0805.2152 [hep-ph]].

[38] V. Hirschi, R. Frederix, S. Frixione, M. V. Garzelli, F. Maltoni and R. Pittau, JHEP **1105**, 044 (2011) [arXiv:1103.0621 [hep-ph]].

[39] G. Cullen, N. Greiner, G. Heinrich, G. Luisoni, P. Mastrolia, G. Ossola, T. Reiter and F. Tramontano, ÂăÂăarXiv:1111.2034 [hep-ph]. ÂăÂă

[40] A. Denner, S. Dittmaier, M. Roth and L. H. Wieders, Nucl. Phys. B **724**, 247 (2005) [arXiv:hep-ph/0505042].

[41] A. Denner, S. Dittmaier, M. Roth and L. H. Wieders, Phys. Lett. B **612**, 223 (2005) [arXiv:hep-ph/0502063].

[42] T. Schutzmeier, "SME reductions in automated NLO computations with NLOX", in preparation.

[43] G. Passarino and M. J. G. Veltman, Nucl. Phys. B **160**, 151 (1979).

[44] A. Denner and S. Dittmaier, Nucl. Phys. B **734**, 62 (2006) [arXiv:hep-ph/0509141].

[45] D. H. Bailey, http://crd.lbl.gov/ dhbailey/mpdist/

[46] T. Diakonidis, J. Fleischer, J. Gluza, K. Kajda, T. Riemann and J. B. Tausk, Phys. Rev. D **80**, 036003 (2009) [arXiv:0812.2134 [hep-ph]].

[47] T. Diakonidis, J. Fleischer, J. Gluza, K. Kajda, T. Riemann and J. B. Tausk, Nucl. Phys. Proc. Suppl. **183**, 109 (2008) [arXiv:0807.2984 [hep-ph]].

[48] R. K. Ellis and G. Zanderighi, JHEP **0802**, 002 (2008) [arXiv:0712.1851 [hep-ph]].

[49] T. Hahn and M. Perez-Victoria, Comput. Phys. Commun. **118**, 153 (1999) [arXiv:hep-ph/9807565].

[50] C. F. Berger *et al.*, [arXiv:0808.0941 [hep-ph]].

[51] H. Hartanto, L. Reina and T. Schutzmeier, in preparation

[52] A. Denner and S. Dittmaier, Nucl. Phys. B **658** (2003) 175 [arXiv:hep-ph/0212259].